Computational Mechanics 21 (1998) 223–235 © Springer-Verlag 1998

A local boundary integral equation (LBIE) method in computational mechanics, and a meshless discretization approach

T. Zhu, J.-D. Zhang, S. N. Atluri

Abstract The Galerkin finite element method (GFEM) owes its popularity to the local nature of nodal basis functions, i.e., the nodal basis function, when viewed globally, is non-zero only over a patch of elements connecting the node in question to its immediately neighboring nodes. The boundary element method (BEM), on the other hand, reduces the dimensionality of the problem by one, through involving the trial functions and their derivatives, only in the integrals over the global boundary of the domain; whereas, the GFEM involves the integration of the "energy" corresponding to the trial function over a patch of elements immediately surrounding the node. The GFEM leads to banded, sparse and symmetric matrices; the BEM based on the global boundary integral equation (GBIE) leads to full and unsymmetrical matrices. Because of the seemingly insurmountable difficulties associated with the automatic generation of element-meshes in GFEM, especially for 3-D problems, there has been a considerable interest in element free Galerkin methods (EFGM) in recent literature. However, the EFGMs still involve domain integrals over shadow elements and lead to difficulties in enforcing essential boundary conditions and in treating nonlinear problems.

The object of the present paper is to present a new method that combines the advantageous features of all the three methods: GFEM, BEM and EFGM. It is a meshless method. It involves only boundary integration, however, over a local boundary centered at the node in question; it poses no difficulties in satisfying essential boundary conditions; it leads to banded and sparse system matrices; it uses the moving least squares (MLS) approximations. The method is based on a Local Boundary Integral Equation (LBIE) approach, which is quite general and easily applicable to nonlinear problems, and non-homogeneous domains.

The concept of a "companion solution" is introduced so that the LBIE for the value of trial solution at the source point, inside the domain Ω of the given problem, involves only the trial function in the integral over the local boundary $\partial\Omega_s$ of a sub-domain Ω_s centered at the node in question. This is in contrast to the traditional GBIE which involves the trial function as well as its gradient over the global boundary Γ of Ω. For source points that lie on Γ, the integrals over $\partial\Omega_s$ involve, on the other hand, both the trial function and its gradient. It is shown that the satisfaction of the essential as well as natural boundary conditions is quite simple and algorithmically very efficient in the present LBIE approach.

In the example problems dealing with Laplace and Poisson's equations, high rates of convergence for the Sobolev norms $||\cdot||_0$ and $||\cdot||_1$ have been found.

In essence, the present EF-LBIE (Element Free-Local Boundary Integral Equation) approach is found to be a simple, efficient, and attractive alternative to the EFG methods that have been extensively popularized in recent literature.

1 Introduction

The meshless discretization approach for continuum mechanics problems has attracted much attention during the past decade. The initial idea dates back to the smooth particle hydrodynamics (SPH) method for modeling astrophysical phenomena (Lucy 1977). By focusing only on the points, instead of the meshed elements as in the conventional finite element method, the meshless approach possesses certain advantages in handling problems with discontinuities, and in numerical discretization of 3-D problems for which automatic mesh generation is still an art in its infancy.

Based upon the general weak formulations, the Galerkin finite element method (GFEM), and the global boundary integral equation (GBIE) which leads to the boundary element method (BEM), can be established (Zhang and Atluri 1986). The Galerkin finite element method, due to its profound roots in generalized variational principles and its ease of use, has found extensive engineering acceptance as well as a commercial market. The typical feature of the finite element method is the sub-domain discretization, and the use of local interpolation functions. Compared to its convenience and flexibility in use, the finite element method has been plagued for a long time by such inherent problems as locking, poor derivative solutions, etc. In contrast, although only a boundary discretization is necessary for linear boundary value problems, the

Communicated by G. Yagawa, 27 July 1997

T. Zhu, J.-D. Zhang, S. N. Atluri
Computational Mechanics Center,
Georgia Institute of Technology,
Atlanta, GA 30332-0356, USA

Correspondence to: T. Zhu

This work was supported by research grants from the Office of Naval Research, and the Federal Aviation Administration, with Y. D. S. Rajapakse, and C. C. Seher as cognizant program officials.

boundary element method is restricted to the cases where the infinite space fundamental solution for the differential operator of the problem must be available. Besides, in the BEM based on the GBIE, the evaluation of the unknown function and/or its gradients at any single point within the domain of the problem involves the calculation of integrals over the entire global boundary, which is tedious and inefficient. In solving the nonlinear problems, both FEM and BEM inevitably have to deal with the nonlinear terms in the domain of the problem, for which the accuracy of the gradient calculation would play a dominant role in terms of convergence. Both methods may become inefficient in solving the problems with discontinuities such as crack propagation (along yet to be determined paths) analysis or the formation of shock waves in fluid dynamic problems.

An alternative option for such problems is the meshless discretization or a finite point discretization approach. The current developments of meshless methods in literature, such as the diffuse element method (Nayroles et al. 1992), the element free Galerkin method (Belytschko et al. 1994, 1995; Krysl et al. 1995; Organ et al. 1996), the reproducing kernel particle method (Liu et al. 1996), and the free mesh method (Yagawa and Yamada 1996), are generally based upon variational formulations. Only very limited improvements have been achieved by the EFG method, when compared to the FEM, in solving discontinuous problems, as both of them are based on the Galerkin formulation, and domain integrals are necessary in constructing the numerical models for the problem. Besides, the integration schemes in the neighborhood of the discontinuity, and the enforcement of essential boundary conditions, are very cumbersome in the EFG method. Due to the non-interpolative MLS approximation and the non-polynomial shape functions for the MLS approximation, the essential boundary conditions in the EFG method, based on the MLS approximation, can not be easily and directly enforced.

It may be seen in the following discussion that the presently proposed method possesses the advantages of finite element and boundary element approaches as well as of the meshless finite point discretization. An efficient and flexible meshless formulation based on the local boundary integral equation (LBIE) is proposed in the current research. The local boundary integral equation is used to represent the values of the unknown function at the point of interest, and may involve the values at those points located inside the domain of influence of the point in question. In this formulation, the requirements for the continuity of the trial function used in an approximation may be greatly relaxed, and no derivatives of the shape functions are needed in constructing the system stiffness matrix, at least for the internal nodes. The essential boundary conditions can be directly and easily enforced even when a non-interpolative approximation of the MLS type is used. The differences between the present method and the conventional boundary integral method, lie in the discretization scheme used and in the technique in constructing the system equations. The present method is also more flexible and easier in dealing with nonlinear problems than the conventional boundary integral equation method. Although mainly 2-D problems described by a harmonic operator are considered in the present paper for illustrative purposes only, the method can be easily applied to elasticity as well as other multi-dimensional linear and nonlinear boundary value problems.

In the present paper, by "the support of a source point (node) $\mathbf{y}_i$" we mean a sub-domain (usually taken as a circle of radius r_i) in which the weight function w_i in the MLS approximation, associated with node $\mathbf{y}_i$, is non-zero; by "the domain of definition" of an MLS approximation for the trial function at any point $\mathbf{x}$ we mean a sub-domain which covers all the nodes whose weight functions do not vanish at $\mathbf{x}$; and by "the domain of influence of node $\mathbf{y}_i$" we denote a sub-domain in which all the nodes have non-zero couplings with the nodal values at $\mathbf{y}_i$, in the system stiffness matrix. The domain of influence of a node is somewhat like a patch of elements in the FEM, which share the node in question. In our implementation, the domain of influence of a node is the union of the domains of definition of the MLS approximation for the trial function at all points on the local boundary of the source point (node). We do not intend to mean these to be versatile definitions, but rather, explanations of our terminology.

The following discussion begins with the description of the local boundary integral equation (LBIE) formulation in Sect. 2. A brief discussion of the approximation or interpolation method is given in Sect. 3. In Sect. 4, the discretization and numerical implementation for this method are presented. A simple comparison between the present method and conventional finite element method is made in Sect. 5 and numerical examples for 2-D potential problems are given in Sect. 6. The paper ends with conclusions and discussions in Sect. 7.

2
Local boundary integral equation

Although the present approach is fully general in solving nonlinear boundary value problems, only the linear Poisson's equation is used in the following, to demonstrate the formulation. The Poisson's equation may be written as

$$\nabla^2 u(\mathbf{x}) = p(\mathbf{x}) \quad \mathbf{x} \in \Omega \tag{1}$$

where p is a given source function, and the domain Ω is enclosed by $\Gamma = \Gamma_u \cup \Gamma_q$, with boundary conditions

$$u = \overline{u} \quad \text{on} \quad \Gamma_u \ , \tag{2a}$$

$$\frac{\partial u}{\partial n} \equiv q = \overline{q} \qquad \text{on} \quad \Gamma_q \tag{2b}$$

where $\overline{u}$ and $\overline{q}$ are the prescribed potential and normal flux, respectively, on the essential boundary Γ_u and on the flux boundary Γ_q, and n is the outward normal direction to the boundary Γ.

A weak formulation of the problem may be written as,

$$\int_\Omega u^* (\nabla^2 u - p)\, \mathrm{d}\Omega = 0 \tag{3}$$

where u^* is the test function and u is the trial function. If one uses the test function which satisfies the equation:

$$\nabla^2 u^*(\mathbf{x}, \mathbf{y}) + \delta(\mathbf{x}, \mathbf{y}) = 0 \tag{4}$$

where $\delta(\mathbf{x},\mathbf{y})$ is the Dirac delta function, after integration by parts twice, the following integral equation can be obtained

$$u(\mathbf{y}) = \int_\Gamma u^*(\mathbf{x},\mathbf{y})\frac{\partial u(\mathbf{x})}{\partial n}\,\mathrm{d}\Gamma - \int_\Gamma u(\mathbf{x})\frac{\partial u^*(\mathbf{x},\mathbf{y})}{\partial n}\,\mathrm{d}\Gamma - \int_\Omega u^* p\,\mathrm{d}\Omega \tag{5}$$

where n is the unit outward normal to the boundary Γ, $\mathbf{x}$ is the generic point and $\mathbf{y}$ is the source point. It is well known from the potential theory that such an integral representation should hold over the entire domain Ω and on its boundary. Even though $\mathbf{y}$ may be a source point within Ω, we label Eq. (5) as the Global Boundary Integral Equation (GBIE). By taking the point $\mathbf{y}$ to the boundary and using the boundary conditions and proper numerical discretization, the formulation leads to the conventional boundary integral equation (and hence, the boundary element) method.

It should be noted that such an integral equation can be considered as an equation to calculate the value of the unknown variable u at the source point $\mathbf{y}$.

If, instead of the entire domain Ω of the given problem, we consider a sub-domain Ω_s, which is located entirely inside Ω and contains the point $\mathbf{y}$, clearly the following equation should also hold over the sub-domain Ω_s:

$$u(\mathbf{y}) = \int_{\partial\Omega_s} u^*(\mathbf{x},\mathbf{y})\frac{\partial u(\mathbf{x})}{\partial n}\,\mathrm{d}\Gamma - \int_{\partial\Omega_s} u(\mathbf{x})\frac{\partial u^*(\mathbf{x},\mathbf{y})}{\partial n}\,\mathrm{d}\Gamma - \int_{\Omega_s} u^* p\,\mathrm{d}\Omega \tag{6}$$

where $\partial\Omega_s$ is the boundary of the sub-domain Ω_s. In other words, the equation for the value of the unknown function at the source point can be obtained by carrying out the integrals over any closed boundary surrounding the point, and over the sub-domain enclosed within the closed boundary.

In the original boundary value problem, either the potential u or the flux $\partial u/\partial n$ may be specified at every point on the global boundary Γ, which makes the integral equation (5) a well posed problem. But none of them is known a priori along the local boundary $\partial\Omega_s$. Especially, the gradient of the unknown function u along the local boundary appears in the integral. In order to get rid of the gradient term in the integral over $\partial\Omega_s$, the concept of a "companion solution" is now introduced into the formulation. The companion solution is associated with the fundamental solution and is defined as the solution of the following Dirichlet problem over the sub-domain Ω_s,

$$\begin{aligned} &\nabla^2 u' = 0 \quad \text{on} \quad \Omega_s, \\ &u' = u^*(\mathbf{x},\mathbf{y}) \quad \text{on} \quad \partial\Omega_s \ . \end{aligned} \tag{7}$$

For $\partial\Omega_s$ located inside Ω note the fact that the fundamental solution u^* is regular everywhere except at the source point $\mathbf{y}$, and hence the solution to the boundary value problem (7) should exist and be regular everywhere in Ω_s.

Using $u^{**} = u^* - u'$ as the test function in the integrals in Eq. (3), and integrating by parts twice yields

$$\begin{aligned} \int_{\Omega_s} -u(\mathbf{x})\nabla^2 u^*(\mathbf{x},\mathbf{y})\mathrm{d}\Omega = &\int_{\partial\Omega_s} u^{**}(\mathbf{x},\mathbf{y})\frac{\partial u(\mathbf{x})}{\partial n}\,\mathrm{d}\Gamma \\ &- \int_{\partial\Omega_s} u(\mathbf{x})\frac{\partial u^{**}(\mathbf{x},\mathbf{y})}{\partial n}\,\mathrm{d}\Gamma \\ &- \int_{\Omega_s} u^{**}(\mathbf{x},\mathbf{y})\,p(\mathbf{x})\,\mathrm{d}\Omega \ . \end{aligned} \tag{8}$$

Noting that $-\nabla^2 u^{**} = -\nabla^2 u^* + \nabla^2 u' = \delta(\mathbf{x},\mathbf{y})$ in Ω_s, and $u^{**} = 0$ along $\partial\Omega_s$, and by the definition of the companion solution, Eq. (8) becomes

$$u(\mathbf{y}) = -\int_{\partial\Omega_s} u(\mathbf{x})\frac{\partial u^{**}(\mathbf{x},\mathbf{y})}{\partial n}\,\mathrm{d}\Gamma - \int_{\Omega_s} u^{**}(\mathbf{x},\mathbf{y})\,p(\mathbf{x})\,\mathrm{d}\Omega \tag{9}$$

for the source point located inside Ω. Thus, only the unknown variable u itself appears in the local boundary integral form. We label Eq. (9) as the Local Boundary Integral Equation (LBIE).

It should be noted that Eq. (9) holds irrespective of the size and shape of $\partial\Omega_s$. This is an important observation which forms the basis for the following development. Also, it is clear that an integral relation similar to that in (9) can be developed for fully nonlinear problems, with the nonlinear terms appearing in the integral over Ω_s. We now deliberately choose a simple regular shape for $\partial\Omega_s$ and thus for Ω_s. The most regular shape of a sub-domain should be an n-dimensional sphere centered at $\mathbf{y}$ for a

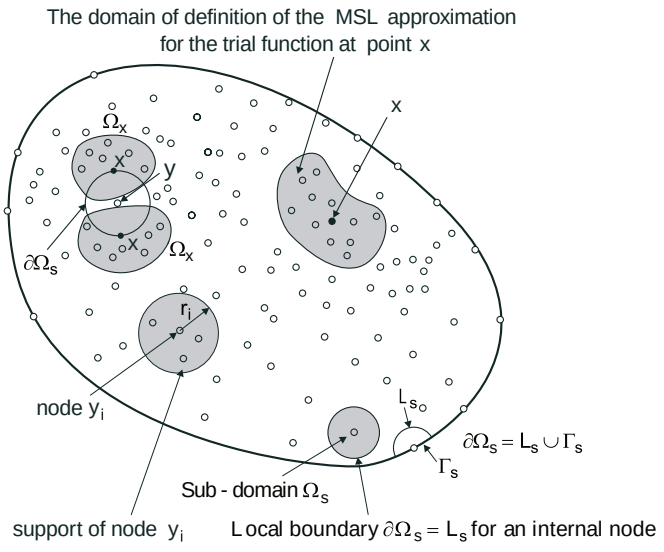

Fig. 1. Local boundaries, the supports of nodes, the domain of definition of the MLS approximation for the trial function at a point, and the domain of influence of a source point (node): (1) The domain of definition of the MSL approximation, $\Omega_{\mathbf{x}}$, for the trial function at any point $\mathbf{x}$ is the domain over which the MLS is defined, i.e., $\Omega_{\mathbf{x}}$ covers all the nodes whose weight functions do not vanish at $\mathbf{x}$. (2) The domain of influence for source point $\mathbf{y}$ is the union of all $\Omega_{\mathbf{x}}, \forall\mathbf{x}$ on $\partial\Omega_s$ (taken to be a circle of radius r_0 in this paper). (3) The support of source point $\mathbf{y}_i$ is a sub-domain (taken to be a circle of radius r_i for convenience) in which the weight function w_i corresponding to this node is non-zero. Note that the "support" of $\mathbf{y}_i$ is distinct and different from the "domain" of influence of $\mathbf{y}_i$

boundary value problem defined on an n-dimensional space (or any other shape can be used for the convenience of solving the specific problem). Over this regular shape, the companion solution u' can be easily and analytically solved for most differential operators for which the fundamental solutions are available. For the current 2-D potential problem, the sub-domain Ω_s is a circle of radius r_0. For the 2-D harmonic operator, the fundamental solution u^* for a 2-D potential operator is given by

$$u^* = -\frac{1}{2\pi}\ln r \tag{10}$$

and hence the companion solution to Eq. (7) over the circle is a constant and given by

$$u' = -\frac{1}{2\pi}\ln r_0 \ . \tag{11}$$

Therefore, the modified test function becomes

$$u^{**} = u^* - u' = \frac{1}{2\pi}\ln\frac{r_0}{r} \tag{12}$$

where $r = |\mathbf{x} - \mathbf{y}|$, and r_0 is the radius of the local sub-domain, Ω_s.

When the source point is located at the global boundary Γ of the original boundary value problem, the sub-domain can still be taken as a part of a circular domain centered at the nodal point, so as to define the companion solution, and the integral boundary should go through the part of the circle located inside the domain Ω and the piece of boundary line Γ_s on which the nodal point in question falls (see Fig. 1). It should be noted that along the piece of boundary line Γ_s, the modified fundamental solution $u^* - u'$, or the integral kernel corresponding to the gradient terms, is not zero anymore. The integral governing a nodal point that lies on the global boundary Γ may become

$$\begin{aligned}\alpha(\mathbf{y})\boldsymbol{u}(\mathbf{y}) = &-\int_{\partial\Omega_s} u(\mathbf{x})\frac{\partial u^{**}(\mathbf{x},\mathbf{y})}{\partial n}\,\mathrm{d}\Gamma \\ &+\int_{\Gamma_s}\frac{\partial u(\mathbf{x})}{\partial n}u^{**}(\mathbf{x},\mathbf{y})\,\mathrm{d}\Gamma \\ &-\int_{\Omega_s} u^{**}(\mathbf{x},\mathbf{y})p(\mathbf{x})\,\mathrm{d}\Omega\end{aligned} \tag{13}$$

where $\alpha(\mathbf{y})$ can be defined by Eq. (30a), such that the flux/traction boundary conditions can be taken into account.

With Eq. (9) and/or Eq. (13) for any source point $\mathbf{y}$, the problem becomes one as if we are dealing with a localized boundary value problem over an n-dimensional sphere Ω_s. The radius of the sphere should not affect the solution except that the companion solution in the integral kernel would vary with the radius. Also, it should be noted that the companion solution is a function of source point $\mathbf{y}$. The remaining problem is how to represent the values of the unknown function on the local boundary $\partial\Omega_s$ such that it can be calculated at the source point, i.e., some appropriate approximation or interpolation scheme has to be invoked. This is the main topic discussed in the next section.

3 Approximation or interpolation schemes for values in Ω_s and on $\partial\Omega_s$

A variety of local interpolation schemes that interpolate the data at randomly scattered points in two or more independent variables are available. These methods have gained more interest in the field of computer aided geometrical design. They range from some very basic formulations to some extremely complicated ones with considerable computational costs.

For computational mechanics problems, different interpolative approaches are feasible. In the finite element method, the interpolation is over the element domain locally or, when viewed globally, the interpolation function is nonzero only over a patch of elements that share the node in question, which may affect the rate of convergence due to the fact that the test and trial functions are chosen from the same functional space. In the traditional boundary element method based on the GBIE, the interpolation function has to involve the values at the global boundary Γ of the problem domain in order to calculate the unknowns at a single point although the interpolation over boundary is piecewise, and is local.

As seen from (13), in the present Local Boundary Integral Equation (LBIE) method, the solution at the source point $\mathbf{y}$ is determined from an integral of the data over a local boundary $\partial\Omega_s$ for $u(\mathbf{x})$ and $\partial u(\mathbf{x})/\partial n$. These boundary data will be interpolated using the nodal values $\mathbf{u}$ at a finite number of points that are arbitrary located within a local domain. Hence the present approach is a "meshless discretization approach".

In order to make the current formulation fully general, it needs a relatively direct *local* interpolation or approximation scheme with reasonably high accuracy, and with ease of extension to n-dimensional problems. The moving least squares approximation is used in the current work for the Poisson's equation. A different choice may be a local non-moving least squares approximation. A brief summary of the MLS and the local least squares approximation schemes is given in the following.

Consider a sub-domain $\Omega_{\mathbf{x}}$, the neighborhood of a point $\mathbf{x}$, which is located in the problem domain Ω. To approximate the distribution of function u in $\Omega_{\mathbf{x}}$, over a number of randomly located nodes $\{\mathbf{x}_i\}$, $i = 1, 2, \ldots, n$, the Moving Least Squares approximant $u^h(\mathbf{x})$ of u, $\forall\mathbf{x} \in \Omega_{\mathbf{x}}$, can be defined by

$$u^h(\mathbf{x}) = \mathbf{p}^T(\mathbf{x})\,\mathbf{a}(\mathbf{x}) \qquad \forall\mathbf{x} \in \Omega_{\mathbf{x}}; \qquad \mathbf{x} = \left[x^1, x^2, x^3\right]^T \tag{14}$$

where $\mathbf{p}^T(\mathbf{x}) = [p_1(\mathbf{x}), p_2(\mathbf{x}), \ldots, p_m(\mathbf{x})]$ is a complete monomial basis of order m; and $\mathbf{a}(\mathbf{x})$ is a vector containing coefficients $a_j(\mathbf{x})$, $j = 1, 2, \ldots, m$ which are functions of the space coordinates $\mathbf{x} = [x^1, x^2, x^3]^T$. For example, for a 2-D problem,

$$\mathbf{p}^T(\mathbf{x}) = [1, x^1, x^2], \qquad \text{linear basis;} \quad m = 3 \ ; \tag{15a}$$

$$\mathbf{p}^T(\mathbf{x}) = [1, x^1, x^2, (x^1)^2, x^1x^2, (x^2)^2], \quad \text{quadratic basis;} \quad m = 6 \ . \tag{15b}$$

The coefficient vector $\mathbf{a}(\mathbf{x})$ is determined by minimizing a weighted discrete L_2 norm, defined as:

$$J(\mathbf{x}) = \sum_{i=1}^{n} w_i(\mathbf{x}) \left[\mathbf{p}^T(\mathbf{x}_i)\mathbf{a}(\mathbf{x}) - \hat{u}_i\right]^2$$
$$= \left[\mathbf{P}\cdot\mathbf{a}(\mathbf{x}) - \hat{\mathbf{u}}\right]^T \cdot \mathbf{W} \cdot \left[\mathbf{P}\cdot\mathbf{a}(\mathbf{x}) - \hat{\mathbf{u}}\right] \quad (16)$$

where $w_i(\mathbf{x})$ is the weight function associated with node i, with $w_i(\mathbf{x}) > 0$ for all $\mathbf{x}$ in the support of $w_i(\mathbf{x})$, $\mathbf{x}_i$ denotes the value of $\mathbf{x}$ at node i, n is the number of nodes in $\Omega_{\mathbf{x}}$ for which the weight functions $w_i(\mathbf{x}) > 0$, and the matrices $\mathbf{P}$ and $\mathbf{W}$ are defined as

$$\mathbf{P} = \begin{bmatrix} \mathbf{p}^T(\mathbf{x}_1) \\ \mathbf{p}^T(\mathbf{x}_2) \\ \cdots \\ \mathbf{p}^T(\mathbf{x}_n) \end{bmatrix}_{n\times m}, \quad (17)$$

$$\mathbf{W} = \begin{bmatrix} w_1(\mathbf{x}) & \cdots & \mathbf{0} \\ \cdots & \cdots & \cdots \\ \mathbf{0} & \cdots & w_n(\mathbf{x}) \end{bmatrix}, \quad (18)$$

and

$$\hat{\mathbf{u}}^T = [\hat{u}_1, \hat{u}_2, \ldots, \hat{u}_n] \ . \quad (19)$$

Here it should be noted that $\hat{u}_i, i = 1, 2, \ldots, n$ in Eqs. (16) and (19) are the fictitious nodal values, and not the nodal values of the unknown trial function $u^h(\mathbf{x})$ in general (see Fig. 2 for a simple one dimensional case for the distinction between u_i and $\hat{u}_i$).

The stationarity of J in Eq. (16) with respect to $\mathbf{a}(\mathbf{x})$ leads to the following linear relation between $\mathbf{a}(\mathbf{x})$ and $\hat{\mathbf{u}}$.

$$\mathbf{A}(\mathbf{x})\mathbf{a}(\mathbf{x}) = \mathbf{B}(\mathbf{x})\,\hat{\mathbf{u}} \quad (20)$$

where matrices $\mathbf{A}(\mathbf{x})$ and $\mathbf{B}(\mathbf{x})$ are defined by

$$\mathbf{A}(\mathbf{x}) = \mathbf{P}^T\mathbf{W}\mathbf{P} = \mathbf{B}(\mathbf{x})\mathbf{P} = \sum_{i=1}^{n} w_i(\mathbf{x})\mathbf{p}(\mathbf{x}_i)\mathbf{p}^T(\mathbf{x}_i) \ , \quad (21)$$

$$\mathbf{B}(\mathbf{x}) = \mathbf{P}^T\mathbf{W}$$
$$= [w_1(\mathbf{x})\,\mathbf{p}(\mathbf{x}_1),\ w_2(\mathbf{x})\,\mathbf{p}(\mathbf{x}_2), \ldots, w_n(\mathbf{x})\,\mathbf{p}(\mathbf{x}_n)] \ . \quad (22)$$

The MLS approximation is well defined only when the matrix $\mathbf{A}$ in Eq. (20) is non-singular. It can be seen that this is the case if and only if the rank of $\mathbf{P}$ equals m. A necessary condition for a well-defined MLS approximation is that at least m weight functions are non-zero (i.e. $n \geq m$) for each sample point $\mathbf{x} \in \Omega$ and that the nodes in $\Omega_{\mathbf{x}}$ will not be arranged in a special pattern such as on a straight line. Here a sample point may be a nodal point under consideration or a quadrature point.

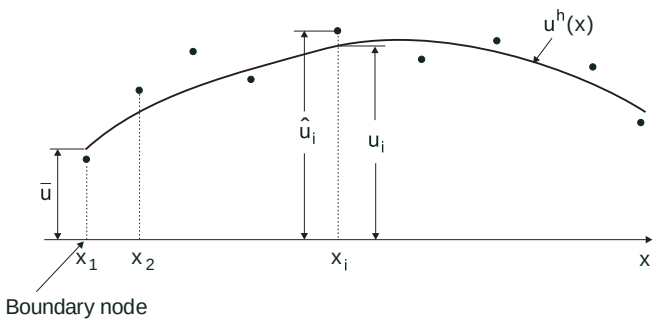

Fig. 2. The distinction between u_i and $\hat{u}_i$

Solving for $\mathbf{a}(\mathbf{x})$ from Eq. (20) and substituting it into Eq. (14) gives a relation which may be written as the form of an interpolation function similar to that used in the FEM, as

$$u^h(\mathbf{x}) = \ \mathbf{\Phi}^T(\mathbf{x}) \cdot \hat{\mathbf{u}} = \sum_{i=1}^{n} \phi_i(\mathbf{x})\hat{u}_i; \quad (23)$$
$$u^h(\mathbf{x}_i) \equiv u_i \neq \hat{u}_i; \qquad \mathbf{x} \in \Omega_{\mathbf{x}}$$

where

$$\mathbf{\Phi}^T(\mathbf{x}) = \mathbf{p}^T(\mathbf{x})\mathbf{A}^{-1}(\mathbf{x})\mathbf{B}(\mathbf{x}) \quad (24)$$

or

$$\phi_i(\mathbf{x}) = \sum_{j=1}^{m} p_j(\mathbf{x})[\mathbf{A}^{-1}(\mathbf{x})\mathbf{B}(\mathbf{x})]_{ji} \ . \quad (25)$$

$\phi_i(\mathbf{x})$ is usually called the shape function of the MLS approximation, corresponding to nodal point $\mathbf{y}_i$. From Eqs. (22) and (25), it may be seen that $\phi_i(\mathbf{x}) = 0$ when $w_i(\mathbf{x}) = 0$. In practical applications, $w_i(\mathbf{x})$ is generally chosen such that it is non-zero over the support of nodal point $\mathbf{y}_i$. The support of the nodal point $\mathbf{y}_i$ is usually taken to be a circle of radius r_i, centered at $\mathbf{y}_i$. The fact that $\phi_i(\mathbf{x}) = 0$, for $\mathbf{x}$ not in the support of nodal point $\mathbf{y}_i$ preserves the *local character* of the Moving Least Squares approximation.

The fact that the MLS approximation u^h does not interpolate the nodal data, i.e. $u^h(\mathbf{x}_i) \equiv u_i \neq \hat{u}_i$ and $\phi_i(\mathbf{x}_j) \neq \delta_{ij}$ causes a major problem in element free Galerkin formulation (Belytschko et al. 1994), but will not pose any difficulty for the present approach as will be seen in Sect. 4.

The smoothness of the shape functions $\phi_i(\mathbf{x})$ is determined by that of the basis functions and of the weight functions. Let $C^k(\Omega)$ be the space of k-th continuously differentiable functions. If $w_i(\mathbf{x}) \in C^k(\Omega)$ and $p_j(\mathbf{x}) \in C^l(\Omega)$, $i = 1, 2, \ldots, n$; $j = 1, 2, \ldots, m$, then $\phi_i(\mathbf{x}) \in C^r(\Omega)$ with $r = \min(k, l)$.

The partial derivatives of $\phi_i(\mathbf{x})$ are obtained as (Belytschko et al. 1994)

$$\phi_{i,k} = \sum_{j=1}^{m}[p_{j,k}(\mathbf{A}^{-1}\mathbf{B})_{ji} + p_j(\mathbf{A}^{-1}\mathbf{B}_{,k} + \mathbf{A}^{-1}_{,k}\mathbf{B})_{ji}] \quad (26)$$

in which $\mathbf{A}^{-1}_{,k} = (\mathbf{A}^{-1})_{,k}$ represents the derivative of the inverse of $\mathbf{A}$ with respect to x^k, which is given by

$$\mathbf{A}^{-1}_{,k} = -\mathbf{A}^{-1}\mathbf{A}_{,k}\mathbf{A}^{-1} \quad (27)$$

where, $(\cdot)_{,i}$ denotes $\partial(\cdot)/\partial x^i$.

A local least squares approximation is easier and more direct. This approximation will not yield a globally continuous surface and generally can not be used in variational based formulation or Galerkin formulation. In the current research, the following basis functions are used

$$\mathbf{p}^T(\mathbf{x}) = [1, r, r\cos\theta, r\sin\theta, r\cos 2\theta, r\sin 2\theta] \quad (28)$$

where r and θ are the local polar coordinates of a node. The shape functions and their derivatives may also be evaluated by Eqs. (25) and (26) with weight functions being 1 and matrices **A** and **B** constant. The shape functions from this approximation scheme look like tents, linearly varied along direction r, which are very similar to those of finite element methods with linear shape functions. The evaluation of the integrals in Eqs. (9) or (13) becomes easier when this approximation method is used.

Although the order of smoothness of the approximation or shape functions built by the MLS approximation is higher, it should be noted that it is in general not necessary to be so, for using the local boundary integral approach, for which even a C^{-1} trial function can give a pretty satisfactory result as has already been shown in some literature on boundary element techniques (see e.g. Zhang and Atluri 1986).

4
Discretization and numerical implementation

It has been pointed out that the normal gradient of u will not appear in the local boundary integrals after the companion solution is introduced into the integral kernel as far as the source point **y** remains within the global boundary Γ of the original problem; but this is not true for the source points located at the boundary of the original problem. In the latter case, a part of boundary integral involves Γ_s, a section of the global boundary Γ of the original problem domain (see Fig. 1), along which the normal flux of u would also be an independent unknown variable when it is not specified. In the numerical implementation, one may either retain the unknown flux $\partial u/\partial n$ as an independent variable in the final linear equations, or to directly differentiate Eq. (23) to represent the unknown flux. When the unknown flux is retained, a simple interpolation/approximation can be used. Thus both u and its normal gradient at the global boundary may appear in the final linear equations as independent unknown variables. The potential u and its gradients at any internal point may be calculated by using Eq. (9). If the direct differentiation of Eq. (23) is used and the flux will not appear as an independent variable, a rather accurate interpolation/approximation with good approximation for derivatives may be required, and the potential and its derivatives can be calculated by Eq. (23) without bothering to integrate Eq. (9) over the local boundary. In the currently presented numerical implementation, the unknown flux at problem boundary is not kept as an independent variable, and the final linear equations contain only the unknown fictitious nodal values $\hat{\mathbf{u}}$.

Equations (9) and (13) are used to derive the system equations and the right hand side vector. As mentioned before, the radius of the local boundary should not affect the result of numerical solution, and hence the size of each local boundary (here it is taken as a circle) can be chosen to be small enough such that the local boundary of any *internal node* will not intersect with the boundary Γ of the problem domain. Only the local boundary integral associated with a boundary node contains Γ_s, which is a part of the boundary Γ of the original problem domain, and $\Gamma_s = \partial\Omega_s \cap \Gamma$ (see Fig. 1).

Substituting Eq. (23) into Eq. (9) for interior nodes, and Eq. (13) for boundary nodes, imposing boundary conditions on the right hand side for node i, and carrying out the integrals, the following linear equations may be obtained

$$\alpha_i u_i = f'_i + \sum_j^N K'_{ij}\hat{u}_j, \quad i = 1, 2, \ldots, N \tag{29}$$

where N is the total number of nodes in the entire domain Ω, $\alpha_i, i = 1, 2, \ldots, N$ are the constant coefficients depending upon the shape of the global boundary, which are

$$\alpha_i = \begin{cases} 1 & \text{for internal nodes,} \\ 1/2 & \text{for nodes on a smooth boundary,} \\ \theta/(2\pi) & \text{for nodes on boundary corners,} \end{cases} \tag{30a}$$

with θ being the internal angle of the boundary corner, and

$$f'_i = \int_{\Gamma_{sq}} u^{**}\overline{q}\,\mathrm{d}\Gamma - \int_{\Gamma_{su}} \overline{u}\frac{\partial u^{**}}{\partial n}\,\mathrm{d}\Gamma - \int_{\Omega_s} u^{**}p\,\mathrm{d}\Omega\ , \tag{30b}$$

$$K'_{ij} = \int_{\Gamma_{su}} u^{**}\frac{\partial \phi_j(\mathbf{x})}{\partial n}\,\mathrm{d}\Gamma - \int_{\Gamma_{sq}} \phi_j(\mathbf{x})\frac{\partial u^{**}}{\partial n}\,\mathrm{d}\Gamma - \int_{L_s} \phi_j(\mathbf{x})\frac{\partial u^{**}}{\partial n}\,\mathrm{d}\Gamma \tag{30c}$$

in which Γ_{sq} and Γ_{su} are the flux and essential boundary sections of Γ_s with $\Gamma_s = \Gamma_{sq} \cup \Gamma_{su}$, $\overline{u}$ is the prescribed value at Γ_{su}, $\overline{q}$ is the prescribed flux at Γ_{sq}, and L_s is a part of the local boundary $\partial\Omega_s$ which is not located on the global boundary Γ. For those interior nodes located inside the domain Ω, $L_s \equiv \partial\Omega_s$, and the boundary integrals involving Γ_{su} and Γ_{sq} vanish in Eqs. (30b) and (30c).

Here, it should be noted that since the value of unknown variable u at the source point **y** (or more precisely, the nodal value of $u^h(\mathbf{x})$ itself) appears on the left hand side of Eq. (29) it is very convenient to impose the essential boundary conditions. On the other hand, this has caused a serious problem for Galerkin-based meshless formulations (Belytschko et al. 1994) due to the fact that only fictitious nodal values instead of nodal values of the unknown variable appear in the approximations such as the MLS approximation. Upon imposing the essential boundary condition for u_i in the left hand side of Eq. (29) for those nodes where u is specified; or using Eq. (23) to represent u for those nodes with u unknown, we have the following linear system

$$\mathbf{K}\hat{\mathbf{u}} = \mathbf{f} \tag{31}$$

with the fictitious nodal values $\hat{\mathbf{u}}$ as unknowns, where the entries for **K** and **f** are given by

$$K_{ij} = \begin{cases} -K'_{ij} & \text{for nodes with } u_i \text{ known,} \\ -K'_{ij} + \alpha_i\phi_j(\mathbf{x}_i) & \text{for nodes with } u_i \text{ unknown ,} \end{cases} \tag{32}$$

and

$$f_i = \begin{cases} f_i' + \alpha_i \overline{u}_i & \text{for nodes with } u_i \text{ known,} \\ f_i' & \text{for nodes with } u_i \text{ unknown .} \end{cases} \quad (33)$$

In implementing the MLS approximation for the local boundary integral equation (LBIE) method, the basis functions and weight functions should be chosen at first. Both Gaussian and spline weight functions with compact supports can be considered. The Gaussian weight function corresponding to node i may be written (Belytschko et al. 1994) as

$$w_i(\mathbf{x}) = \begin{cases} \dfrac{\exp[-(d_i/c_i)^{2k}] - \exp[-(r_i/c_i)^{2k}]}{1 - \exp[-(r_i/c_i)^{2k}]} & 0 \le d_i \le r_i, \\ 0 & d_i \ge r_i \end{cases} \quad (34)$$

where $d_i = ||\mathbf{x} - \mathbf{x}_i||$; c_i is a constant controlling the shape of the weight function w_i and therefore the relative weights; and r_i is the size of the support for the weight function w_i and determines the support of node $\mathbf{x}_i$. In the present computation, $k = 1$ was chosen.

A spline weight function is defined as

$$w_i(\mathbf{x}) = \begin{cases} 1 - 6\left(\dfrac{d_i}{r_i}\right)^2 + 8\left(\dfrac{d_i}{r_i}\right)^3 - 3\left(\dfrac{d_i}{r_i}\right)^4 & 0 \le d_i \le r_i, \\ 0 & d_i \ge r_i \ . \end{cases} \quad (35)$$

The size of support, r_i, of the weight function w_i associated with node i should be chosen such that r_i should be large enough to have sufficient number of nodes covered in the domain of definition of the MLS approximation for the trial function at every sample point ($n \ge m$) to ensure the regularity of $\mathbf{A}$. A very small r_i may result a relatively large numerical error in using Gauss numerical quadrature to calculate the entries in the system matrix. On the other hand, r_i should also be small enough to maintain the local character for the MLS approximation.

The implementation of the present method can be carried out according to the following routine,

1. Choose a finite number of points in the domain Ω and on the boundary Γ of the given physical domain; decide the basis functions and weight functions such that the MLS approximation is well defined.
2. Determine the local sub-domain Ω_s and its corresponding local boundary $\partial\Omega_s$ for each node (see Fig. 1).
3. Loop over all nodes located inside the domain and at the boundary
   - Determine Gaussian quadrature points $\mathbf{x}_Q$ in Ω_s and on $\partial\Omega_s$.
   - Loop over quadrature points $\mathbf{x}_Q$ in the sub-domain Ω_s and on the local boundary $\partial\Omega_s$
     (a) determine the nodes $\mathbf{x}_i$ located in the domain of definition of the MLS approximation for the trial function at point $\mathbf{x}_Q$, i.e., those nodes with $w_i(\mathbf{x}_Q) > 0$;
     (b) for those nodes in the domain of definition of the MLS approximation of trial function at point $\mathbf{x}_Q$; calculate $\phi_i(\mathbf{x}_Q)$ and the derivatives $\phi_{i,j}(\mathbf{x}_Q)$ for the nodes with Γ_{su} non-empty;
     (c) evaluate numerical integrals in Eqs. (30b), (30c);
     (d) deal with the left hand side of Eq. (29);
     (e) assemble contributions to the equations for nodes in $\mathbf{K}, \mathbf{f}$;
     (f) end if
   - End quadrature point loop
4. End node loop.
5. Solve the linear system equation for the fictitious nodal values $\hat{\mathbf{u}}$.
6. Calculate the value of the unknown variable and its derivatives by using Eq. (23) at those sample points under consideration.

Also, from Eq. (30c), it is seen that no derivatives of the shape functions are needed in constructing the stiffness matrix for the internal nodes and for those boundary nodes with no essential-boundary-condition-prescribed sections on their local boundaries. This is attractive in engineering applications as the calculation of derivatives of shape functions from the MLS approximation is quite costly.

The locations of the non-zero entries in every line of the system matrix depend upon the nodes located inside the domain of influence of the source nodal point. If the shape and size of the domain of influence for all of the nodal points are taken to be the same as each other, it may be easy to see that the resulting system matrix becomes banded with non-zero entries being symmetrically and sparsely located with unsymmetric values. That is, if node i is located inside the domain of influence of node j, the node j would also located inside the domain of influence of node i. This may provide some convenience in constructing the system matrix. A non-symmetric matrix $\mathbf{K}$ may need more computer memory and computation cost, but the flexibility, ease of implementation and accuracy embodied in the present formulation will still make it attractive. The density of the nodal point distribution may vary, depending upon the local variation of the unknown variable. Thus, even with the same size of the domain of influence for all the nodes, the number of nodal points covered by the domain of influence associated with different nodes may be different, such that the resolution of the numerical solution can be improved by adding more nodes at some place where the unknown variable may have a dramatic variation. There are no mesh lines connected to the nodal points in the discretized model, so that it is easy to implement intelligent, adaptive algorithms in engineering applications.

5 Comparison between the present method and the finite element method

Although the present method uses the local boundary integral formulation to construct the system equations, the method is more like the finite element method in the sense that the present method does not need to keep the unknown flux as an independent variable for the present

Poisson's equation. A simple comparison of the present method with the Galerkin finite element method, for a simple seven node domain, would be of interest to delineate the differences between them.

Consider first a regular domain with the node 1, located at the origin and the six other equally spaced nodes on the unit circle (see Fig. 3, Mesh a). Connecting the six nodes with the node at origin, forms an FEM model with six constant strain triangular elements. The radius of the local boundary for node 1 is $r_0 < 1$. It is found that the coefficients in the system stiffness matrices corresponding to node 1 computed by the present approach with both the MLS and the local least square approximations are:

$$[1, -1/6, -1/6, -1/6, -1/6, -1/6, -1/6] \tag{36}$$

which are identical to the coefficients in the global system matrix corresponding to node 1, generated by the Galerkin FEM (GFEM) with "constant strain triangular elements".

Next if we place the six nodes on the unit circle unevenly along the circle (see Fig. 3, Mesh b), then the line in the stiffness matrix for GFEM becomes

$$[1, -0.1133, -0.1133, -0.1934, -0.1934, -0.1934, -0.1934] \tag{37a}$$

and those using the MLS and local least squares approximations in the present LBIE approach become, respectively

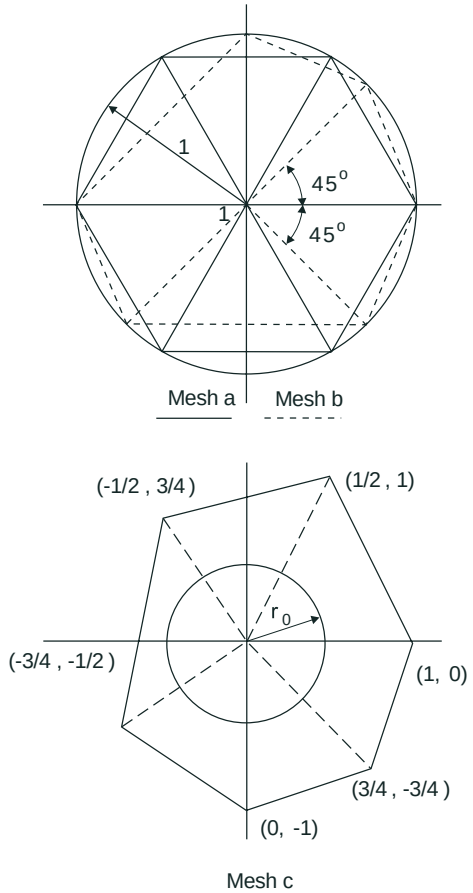

Fig. 3. Comparison with FEM: meshes

$$[1, -0.0940, -0.0940, -0.2325, -0.1735, -0.1735, -0.2325] \ , \tag{37b}$$

$$[1, -0.0732, -0.0732, -0.2500, -0.1768, -0.1768, -0.2500] \ . \tag{37c}$$

It may be seen that those are still relatively comparable to each other.

Finally, if the six nodes are placed randomly (see Fig. 3, Mesh c), it is found that those coefficients become

$$[1, -0.1733, -0.1188, -0.2574, -0.2310, -0.1271, -0.0924] \tag{38a}$$

for the finite element method, and,

$$[1, -0.1638, -0.1256, -0.2424, -0.2613, -0.8067, -0.1209] \ , \tag{38b}$$

$$[1, -0.1914, -0.1101, -0.2541, -0.2446, -0.1143, -0.0855] \tag{38c}$$

for the present LBIE method with the MLS and local least squares approximations, respectively, for $r_0 = 0.1$. We see that, though they are different, they are still comparable to each other.

These simple examples show that the results of numerical discretization based upon the present LBIE method are similar to those of the Galerkin finite element method, even though the present LBIE method uses only the local boundary integral formulation instead of the element domain integration for strain energy as in GFEM. Although, for these simple examples, the local least squares approximation works well, it may not be easily extended to higher dimensional problems and may result unstable solutions for extremely irregular meshes. Therefore in the sequel, the MLS approximation is used in all our numerical examples.

6 Numerical examples

In this section, some numerical results are presented to illustrate the implementation and convergence of the present LBIE approach. For the purpose of error estimation and convergence studies, the Sobolev norms $\|\cdot\|_k$ are calculated. In the following numerical examples, the Sobolev norms for $k = 0$ and $k = 1$ are considered for the present potential problem. These norms are defined as:

$$\|u\|_0 = \left(\int_\Omega u^2 \, \mathrm{d}\Omega \right)^{\frac{1}{2}} \tag{39a}$$

and

$$\|u\|_1 = \left(\int_\Omega u^2 + (|\nabla u|)^2 \, \mathrm{d}\Omega \right)^{\frac{1}{2}} \ . \tag{39b}$$

The relative errors are defined as

$$r_k = \frac{\|u^{\mathrm{num}} - u^{\mathrm{exact}}\|_k}{\|u^{\mathrm{exact}}\|_k}, \qquad k = 0, 1 \ . \tag{40}$$

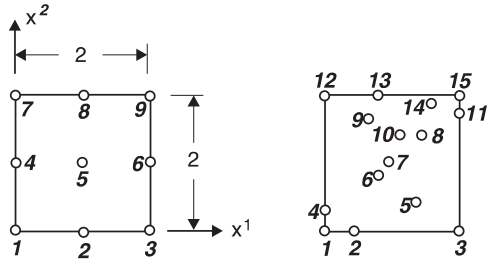

(a) regular nodes (b) irregular nodes

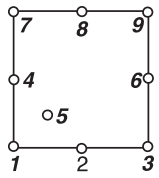

(c) irregular node 5

Coordinates for patch (b)

Nodes	(x^1, x^2)
2	0.3, 0.0
4	0.0, 0.2
5	1.2, 0.4
6	0.8, 0.9
7	0.9, 1.0
8	1.4, 1.2
9	0.5, 1.3
10	1.1, 1.2
11	2.0, 1.8
13	0.8, 2.0
14	1.6, 1.9

Fig. 4. Nodes for the patch test

6.1 Patch test

Consider the standard patch test in a domain of dimension 2×2 as shown in Fig. 4, and a Dirichlet problem with $p = 0$ in Eq. (1) (or the Laplace equation). we consider a problem with the exact solution

$$u = x^1 + x^2 \tag{41}$$

where the potential boundary condition Eq. (2a) is prescribed on all boundaries according to Eq. (41). Satisfaction of the patch test requires that the value of u at any interior node be given by the same linear function (41); and that the derivatives of the computed solution be constant in the patch.

Since the exact solution is linear, a linear basis for the MLS approximation is able to represent this solution. Note that the shape functions and their derivatives from the MLS approximation are no longer piecewise polynomials, and the numerical integration scheme will not yield accurate values for the matrices in the linear system (31). In this example, 9 Gauss points are used on each local boundary L_s (a circle for internal nodes and a part of a circle for boundary nodes in this case), and 6 points are used on each boundary section Γ_s for numerical quadratures.

The nodal arrangements of all patches are shown in Fig. 4. Both Gaussian and spline weight functions are tested. In all cases, $r_i = 4$ and $r_i/c_i = 4$ are used in the computation. In Fig. 4, the coordinates of node 5 for mesh c1, c2, c3, c4, c5 and c6 are (1.1, 1.1), (0.1, 0.1), (0.1, 1.8), (1.9, 1.8), (0.9, 0.9) and (0.3, 0.4) respectively.

The computational results show that the present meshless method based on local boundary integral equation (LBIE) passes all the patch tests in Fig. 4 for both Gaussian and spline weight functions with the given source function $p = 0$.

6.2 Laplace equation

The second example solved here is the Laplace equation in the 2×2 domain shown in Fig. 4, with the exact solution, a cubic polynomial, as

$$u = -(x^1)^3 - (x^2)^3 + 3(x^1)^2 x^2 + 3x^1(x^2)^2 \ . \tag{42}$$

A Dirichlet problem is solved, for which the essential boundary condition is imposed on all sides, and a mixed problem, for which the essential boundary condition is imposed on the top and bottom sides and the flux boundary condition is prescribed on the left and right sides of the domain. The MLS approximation with both linear and quadratic bases as well as Gaussian and spline weight functions are employed in the computation. The size of support for both weight functions are taken to be 2, and the parameter c_i for Gauss weight function is $r_i/4$.

Regular meshes of $9(3 \times 3)$, $36(6 \times 6)$ and $64(8 \times 8)$ nodes are used to study the convergence of the method. The local boundary integrals on $\partial\Omega_s$ are evaluated by using 20 Gauss points on each local boundary. The size (radius) of the local boundary for each node is taken as 0.005 in the computation.

The convergence with mesh refinement of the present method is studied for this problem. The results of relative errors and convergence for norms $\|\cdot\|_0$ and $\|\cdot\|_1$ are shown in Fig. 5 for the Dirichlet problem and in Fig. 6 for the mixed problem, respectively.

It can be seen that the present meshless method based upon the LBIE method has high rates of convergence for norms $||\cdot||_0$ and $\|\cdot\|_1$ and gives reasonably accurate results for the unknown variable and its derivatives.

6.3 Poisson's equation

The results from the present meshless LBIE formulation are also studied for the Poisson's equation with a given source function $p = x^1 + x^2$ in the same 2×2 domain, for which the exact solution is taken to be

$$u = -\tfrac{5}{6}\left[(x^1)^3 + (x^2)^3\right] + 3(x^1)^2 x^2 + 3x^1(x^2)^2 \tag{43}$$

The boundary conditions, the size of local boundary, the parameters c_i and r_i in the MLS approximation as well as the nodal arrangement are the same as those used in the last example. Also, the MLS approximations with both linear and quadratic bases as well as Gaussian and spline weight functions are tested in the computation.

The convergence with mesh refinement of the present method is studied for this problem. The results of relative errors and convergence for the $||\cdot||_0$ and $||\cdot||_1$ norms are shown in Fig. 7 for the Dirichlet problem and in Fig. 8 for the mixed problem, respectively. These figures show that the present meshless method works quite well for the Poisson's equation.

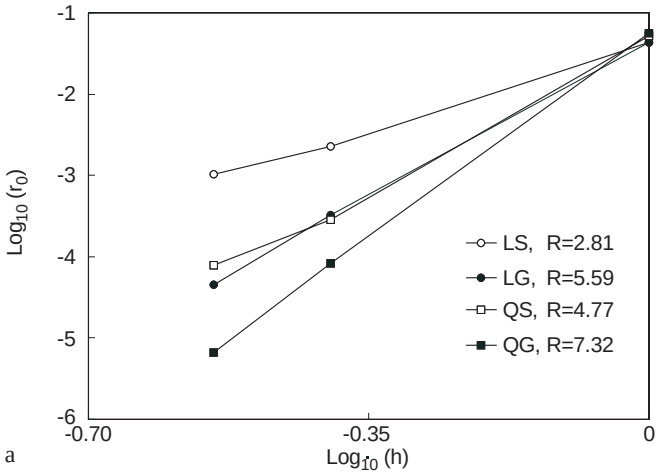

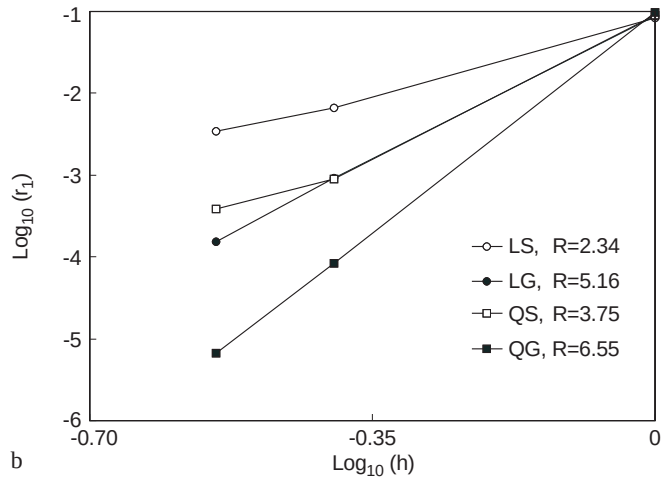

Fig. 5a,b. Relative errors and convergence rates for the *Dirichlet* problem of Laplace equation: **a** for norm $||\cdot||_0$, **b** for norm $||\cdot||_1$. In this figure and thereafter, R is the convergence rate; and "LS", "LG", "QS" and "QG" denote "Linear Spline", "Linear Gaussian", "Quadratic Spline" and "Quadratic Gaussian" respectively

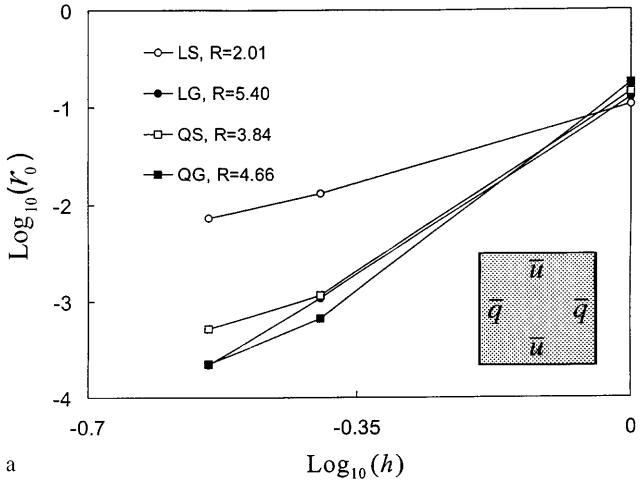

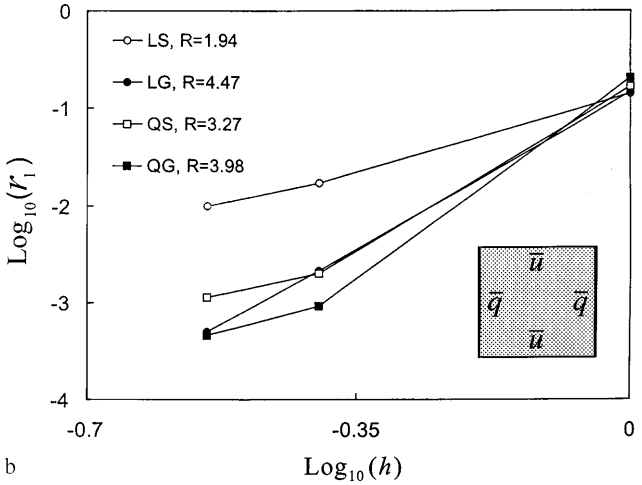

Fig. 6a,b. Relative errors and convergence rates for the *mixed* problem of Laplace equation: **a** for norm $||\cdot||_0$, **b** for norm $||\cdot||_1$

From these two examples, it can be seen that the quadratic basis yields somewhat of a better result than the linear basis while both bases possess high accuracy. Also, the Gauss weight function works better than the spline weight function. We should keep in mind that the appropriate parameters c_i in Eq. (34) need to be determined for all nodes for the Gauss weight function. The values of these parameters will effect the numerical results considerably. With inappropriate c_i used in the Gaussian weight function, the results may become very unsatisfactory. The optimal choice of these parameters is still an open research topic.

6.4 Potential flow

Consider the problem of a potential flow around a cylinder of radius a in an infinite domain, shown in Fig. 9. u represents the stream function.

Due to symmetry, here only a part, $0 \le x^1 \le 4$ and $0 \le x^2 \le 2$, of the upper left quadrant of the field is modeled as shown in Fig. 9. The exact solution for this problem is given by

$$u = x^2\left[1 - \frac{x^1}{(x^2)^2 + (x^1 - L)^2}\right] \quad . \tag{44}$$

Figure 9 shows the prescribed u and $\partial u/\partial n$ values along all boundaries. The essential boundary condition on the left and top edges is imposed according to the exact solution (44).

The initial mesh of 24 nodes is considered as shown in Fig. 10a. Subsequently, the number of nodes is increased to 47 in Fig. 10b and 74 in Fig. 10c to study the convergence of the present meshless method.

Both linear and quadratic bases as well as Gaussian and spline weight functions are considered. We use $c_i = l_i$ and $r_i = 4c_i$ in the calculation, where l_i is defined as (Belytschko et al. 1994)

$$l_i = \max_{j \in S_j} ||\mathbf{x}_j - \mathbf{x}_i|| \tag{45}$$

where S_j is the minimum set of neighboring nodes of $\mathbf{x}_i$ which construct a polygon surrounding $\mathbf{x}_i$.

The convergence for the Sobolev norms $||\cdot||_0$ and $||\cdot||_1$ is shown in Fig. 11. The mesh size h in this problem is defined as the average mesh sizes on the bottom edge. From Fig. 11, we notice that the quadratic basis is sur-

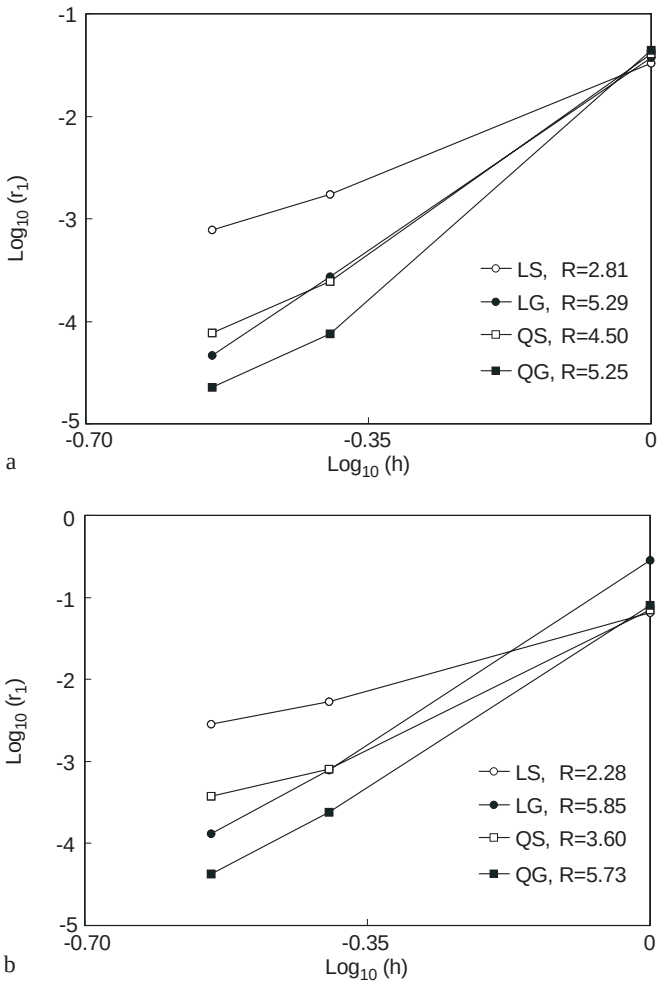

Fig. 7a,b. Relative errors and convergence rates for the *Dirichlet* problem of Poisson's equation: **a** for norm $||\cdot||_0$, **b** for norm $||\cdot||_1$

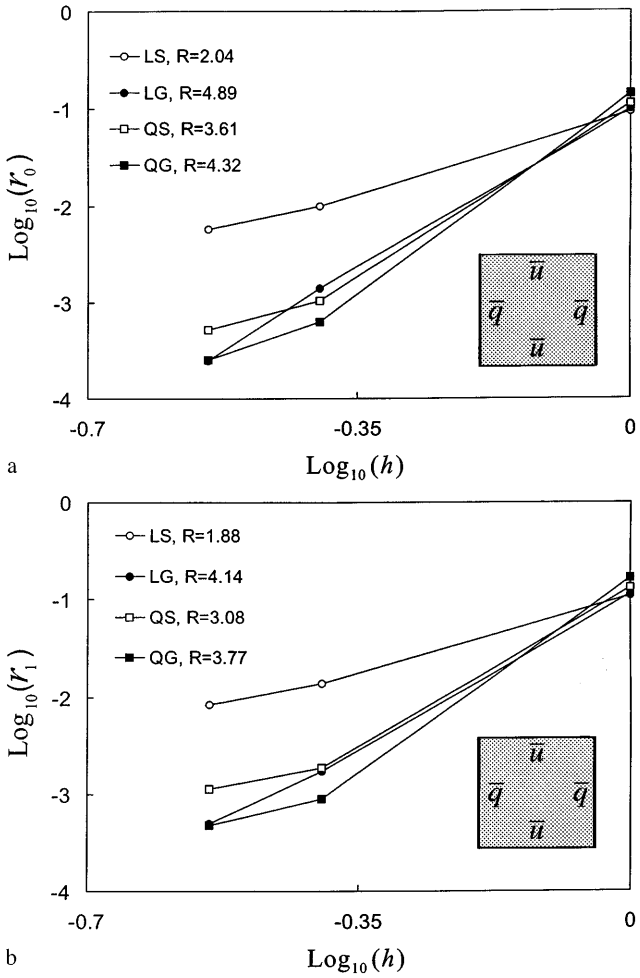

Fig. 8a,b. Relative errors and convergence rates for the *mixed* problem of Poisson's equation: **a** for norm $||\cdot||_0$, **b** for norm $||\cdot||_1$

prisingly not as good as the linear basis in this problem for both Gaussian and spline weight functions.

The stream lines from the exact solution and from the numerical solution of the present meshless formulation with a linear basis and Gaussian weight functions for the cases of 47 and 74 nodes are also shown in Fig. 12. It can be seen that the stream lines are well approximated by the present method with 74 nodes as compared to the closed form solution.

7
Conclusions and discussions

The basic concept and implementation of a local boundary integral equation formulation for solving the boundary value problems have been presented in the present work. The numerical implementation of the approach may lead to an efficient meshless discrete model. The concept of a companion solution is introduced, such that the gradient or derivative terms would not appear in the integrals over the local boundary after the modified integral kernel is used, for all nodes whose local boundary $\partial\Omega_s$ fall within the global boundary $\partial\Omega$ of the given problem. The non-dependence of the solution on the size of the integral local boundary provides a great flexibility in dealing with the numerical model of the boundary value problems. Convergence studies in the numerical examples show that the present method possesses an excellent rate of convergence for both the unknown variable and its derivatives. Only a simple numerical manipulation is needed for calculating the derivatives of the unknown function, as the original approximated trial solution is smooth enough to yield reasonably accurate results for derivatives. The numerical results show that using both linear and quadratic bases as well as spline and Gaussian weight functions in the approximation function can give quite accurate numerical results.

Compared with the other meshless techniques discussed in literature based on Galerkin formulation (for instance, Belytschko et al. 1994; Mukherjee and Mukherjee 1997), the present approach is found to have the following advantages.

- The essential boundary condition can be very easily and directly enforced.
- No special integration scheme is needed to evaluate the volume and boundary integrals. The integrals in the present method are evaluated only over a regular sub-

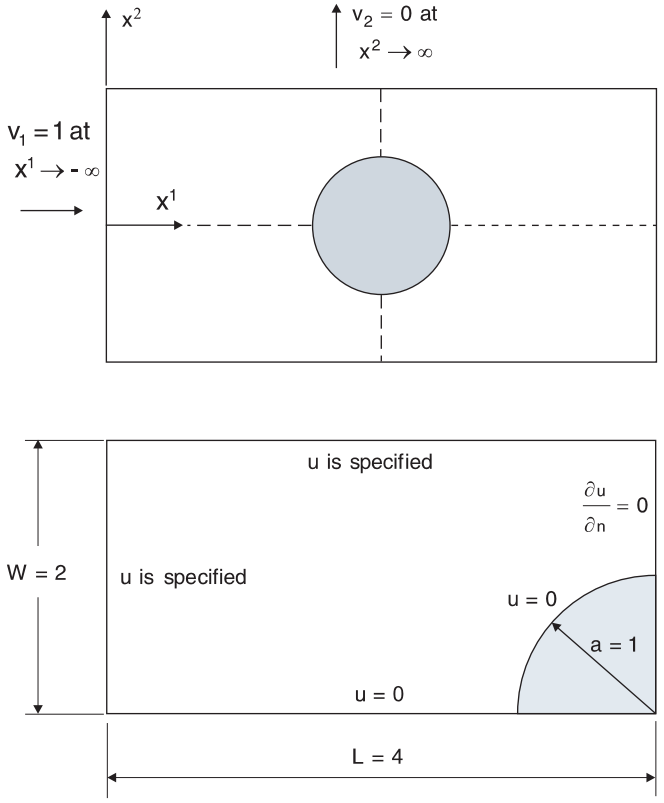

Fig. 9. Flow around a cylinder in an infinite field and the model with boundary conditions

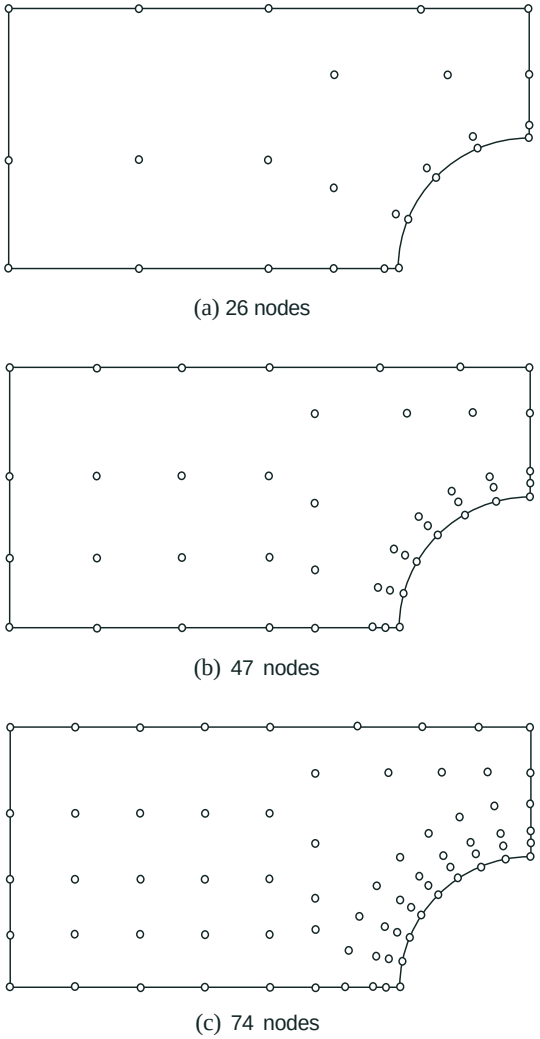

Fig. 10. Flow around a cylinder: nodal arrangement

domain and along a regular boundary surrounding the source point. The local boundary in general is the surface of a "unit sphere" centered at the node in question. This flexibility in choosing the size and the shape of the local boundary will lead to more convenience in dealing with the nonlinear problems.

- Due to the fact that an exact solution (the infinite space fundamental solution) is used as a test function to enforce the weak formulation, a better accuracy may be achieved in numerical calculation.
- No derivatives of shape functions are needed in constructing the system stiffness matrix for the internal nodes, as well as for those boundary nodes with no essential-boundary-condition-prescribed sections on their local integral boundaries.

While the conventional boundary element method is based on the "global" boundary integral equations, the present LBIE formulation is advantageous because:

- The volume integration needs to be carried out only over a small regular sub-domain Ω_s of the problem in dealing with the boundary value problems for which the volume integral has to be present. The same is true for nonlinear problems.
- In the present LBIE method, the unknown variable and its derivatives at any point can be easily calculated from the interpolated/approximated trial solution only over the nodes within the domain of definition of the MSL approximation for the trial function at this point; while this involves an integration through all of the boundary points at the global boundary Γ, in the boundary element method.
- Non-smooth boundary points (corners) cause no problems in the present method, while special attention is needed in the traditional boundary element method to deal with these corner points.
- It is not necessary in general to keep the unknown flux/traction on the boundary as an independent variable for the present method.
- The stiffness matrix is banded in the present method instead of being fully populated in the traditional BEM.

Besides, the current formulation possesses flexibility in adapting the density of the nodal points at any place of the problem domain such that the resolution and fidelity of the solution can be improved easily. This is especially useful in developing intelligent, adaptive algorithms based on error indicators, for engineering applications.

The present method possesses a tremendous potential for solving nonlinear problems and/or problems with discontinuities. Further results in using the current approach in some solid mechanics problems will be presented in a series of forthcoming papers.

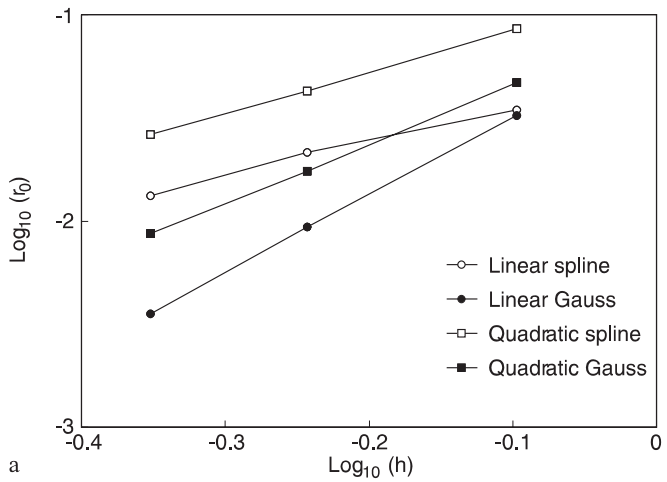

a

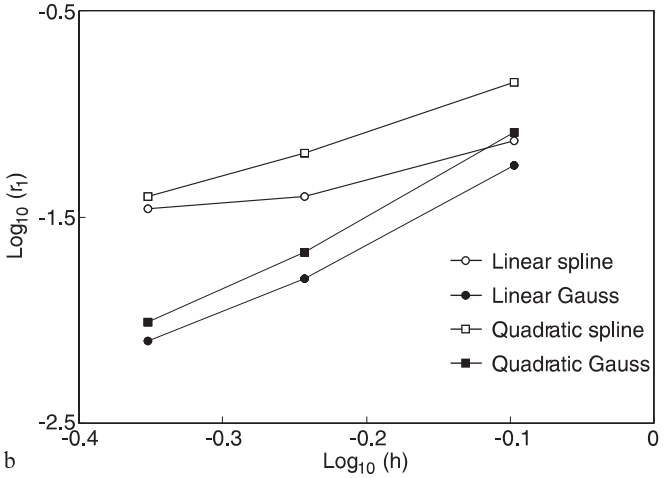

b

Fig. 11a,b. Relative errors and convergence rates for the potential flow problem: **a** for norm $\|\cdot\|_0$, **b** for norm $\|\cdot\|_1$

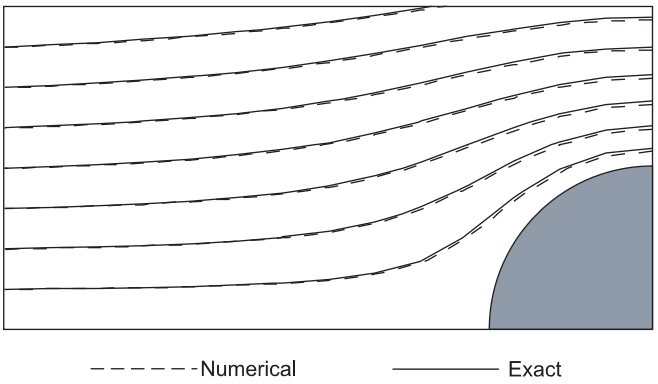

(a) Linear basis, Gaussian weight functions, 47 nodes

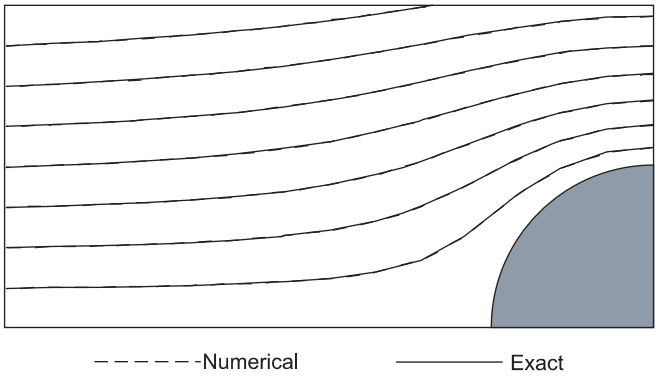

(b) Linear basis, Gaussian weight functions, 74 nodes

Fig. 12. The stream lines of the flow problem

References

Belytschko T, Lu YY, Gu L (1994) Element-free Galerkin methods. Int. J. Num. Meth. Eng. 37:229–256

Belytschko T, Organ D, Krongauz Y (1995) A coupled finite element-element-free Galerkin method. Comput. Mech. 17:186–195

Krysl P, Belytschko T (1995) Analysis of thin plates by the element-free Galerkin methods. Comput. Mech. 17:26–35

Liu WK, Chen Y, Chang CT, Belytschko T (1996) Advances in multiple scale kernel particle methods. Comput. Mech. 18:73–111

Lucy LB (1977) A numerical approach to the testing of the fission hypothesis. The Astro. J. 8(12):1013–1024

Mukherjee YX, Mukherjee S (1997) On boundary conditions in the element-free Galerkin method. Comput. Mech. 19:264–270

Nayroles B, Touzot G, Villon P (1992) Generalizing the finite element method: diffuse approximation and diffuse elements. Comput. Mech. 10:307–318

Organ D, Fleming M, Terry T, Belytschko T (1996) Continuous meshless approximations for nonconvex bodies by diffraction and transparency. Comput. Mech. 18:225–235

Yagawa G, Yamada T (1996) Free mesh method, A new meshless finite element method. Comput. Mech. 18:383–386

Zhang J-D, Atluri SN (1986) A boundary/interior element for the quasi-static and transient response analysis of shallow shells. Comput. Struct. 24:213–214